Growth and electronic properties of Ti nanoislands on Au(111)

P. Carrozzo, F. Tumino, M. Passoni, C.E. Bottani, C.S. Casari *, A. Li Bassi

Dipartimento di Energia and NEMAS, Center for NanoEngineered MAterials and Surfaces, Politecnico di Milano, Via Ponzio 34/3, I-20133, Milan, Italy

Article history:
Received 23 June 2013
Accepted 2 September 2013
Available online 13 September 2013

1. Introduction

Metal clusters supported on solid surfaces constitute a nanostructured surface system with tunable electronic properties. The capability to produce and control these systems has a fundamental relevance for the development of novel surfaces for applications, e.g. in catalysis, optoelectronics and spintronics. In this framework the study of the basic mechanisms which determine the size and structure of single clusters and the related effects on the electronic properties is fundamental.

Titanium has a great importance in the field of model catalysis for its good corrosion-resistance and remarkable activity in many oxidation reactions [1]. To this respect the controlled growth of nanoislands from isolated aggregates to coalescence and up to film formation and the correspondent effect on the electronic properties can be beneficial for the mentioned applications, while, from a fundamental point of view, the control of layers of metallic Ti clusters is a key step for subsequent oxidation into TiO_2. Moreover the capability to select cluster positioning on the surface can add further control for nanoscale applications. To this aim a possible approach is based on the use of specific substrate properties such as preferential nucleation sites for nanoisland formation, as in the case of the Au(111) $22\times\sqrt{3}$ *herringbone reconstruction.* This reconstruction is characterized by fcc and hcp regions that are separated by ridges which can alternatively turn by 120° in correspondence of a change in surface domain orientation generating the so-called elbows [2]. A variety of metals preferentially grow at the elbow sites of such surface forming well-ordered arrays of nanoislands, as in the case of Fe, Co, Ni, Pd, Pt, Mo and Ti [3–9]. Even if all these metals are characterized by preferential nucleation, some relevant differences discriminate their growth. Indeed, a different degree of interaction and intermixing between surface and adlayer can result in the growth of islands with mixed composition even at room temperature (as in the case of nickel [10] and platinum [7]) or, at the other extreme, in the nucleation of gold-free islands (as in the case of iron [3] and palladium [11]). Moreover, during the growth process, the islands can have a different interaction with the substrate in some cases leading to a significant distortion of the Au(111) reconstruction [11,12] and to a modification of the local electronic properties of the surface [13].

Only a few works [9,14] report an analysis of the growth mechanisms and electronic properties of supported titanium islands on Au(111). Biener et al. [9] evaporated titanium on Au(111) at room temperature for subsequent oxidation into TiO_2, showing the formation at low coverage of small monolayer Ti islands which avoid the step edge of the gold surface. Similarly Potapenko et al. [14] showed that a low temperature substrate (room temperature or below) is required to avoid migration of Ti into gold during deposition. These works were mainly focused on the formation of TiO_2 nanocrystals, while neither a complete analysis of Ti growth mechanisms on Au(111) nor a detailed investigation of the electronic properties at the nanoscale is available yet.

Here we focus on a detailed scanning tunneling microscopy and spectroscopy (STM-STS) study of the growth mechanisms of Ti on Au(111) in the sub-monolayer coverage regime. We observe the growth of irregular islands composed of small grains of about 1–2 nm^2. We analyzed the morphological properties as a function of coverage in order to investigate island growth, the occurrence of disordered (out-of-elbow) nucleation and the coalescence threshold among Ti islands, discussing the differences with respect to other metals showing preferential nucleation on Au(111). With the help of a proper diffusive model, we were able to quantify the interlayer diffusion among the first two Ti layers observed

* Corresponding author. Tel.: +39 0223996331; fax: +39 0223996309.
E-mail address: carlo.casari@polimi.it (C.S. Casari).

in the investigated range of coverage. Finally STS spectra and differential conductivity maps of the systems allowed us to characterize the local density of states (LDOS) on titanium islands and their relation with the electronic properties of the gold surface.

2. Experimental details

Scanning Tunneling Microscopy and Spectroscopy (STM-STS) measurements were carried out in an ultrahigh-vacuum (UHV) chamber (base pressure ~5×10^{-11} mbar) equipped with sample preparation facilities and an Omicron VT-SPM. The surface of a Au(111) single crystal (MaTecK GmbH, Germany) was cleaned and prepared in UHV by 15 min Ar^+ sputtering at 1 KeV at a sample temperature of 850 K, which was kept for at least 30 min after the sputtering. A preliminary STM characterization of the clean surface was performed in order to exclude contaminations and check the quality of the $(22\times\sqrt{3})$ reconstruction. Titanium was deposited by means of electron-beam evaporation (Ti wire purity 99.99%) on the clean Au(111) surface kept at room temperature (RT). The deposition rate (about 3.3×10^{-3} ML/s) was controlled by monitoring the ion flux from the evaporator. Even though a great care was used to avoid contaminations a slight oxidation of the Ti deposits cannot be excluded, as shown by photoelectron spectra reported by Biener et al. [9].

The amount of Ti was estimated by a software analysis of STM images. Coverage was varied from 0.05 ML up to 1.00 ML, referring to the total amount of deposited Ti, i.e. considering the contribution of all Ti layers. Morphological properties were studied by means of constant current STM images taken at room temperature at a sample-tip bias voltage in the range from −2 to +2 V and a tunneling current in the range 0.2–2 nA. *dI/dV* spectra were acquired at 100 K by means of a lock-in amplifier applying a modulation of 20 mV at the frequency of 8 kHz. At least five STS spectra were recorded at each point of interest for consistency. To discriminate the influence of the tip in spectroscopic measurements, STS experiments were repeated with two different kinds of tip, namely bulk W and Cr tips. The former one has been prepared by standard electrochemical etching while preparation of bulk Cr tips is described elsewhere [15].

3. Results and discussion

3.1. Morphological properties

STM images in Fig. 1 show the evolution of the initial growth of titanium on Au(111) up to about 1.00 ML coverage. At low coverage (Fig. 1.a) Ti islands preferentially nucleate at the elbows of the herringbone reconstruction (both on the fcc region outside bulged elbows and in the hcp region between the ridges of pinched elbows), generating an initial ordered growth, as observed in previous works [9,14]. However, even at the lowest investigated coverage (0.05 ML), Ti islands saturate all the available elbows and a few islands about 1–2 nm^2 are already present out of these sites, meaning that nucleation at the elbows, although preferred, does not represent the only choice for Ti to nucleate or may be limited by the existence of a critical size beyond which island growth is not favored (see discussion below). In addition, no Ti islands are observed at the Au(111) step edges, up to a distance of about 2–4 nm (not shown), in agreement with previous works [9].

As coverage is increased, Ti islands at the elbows, starting from an average size of about 3.5 nm^2 at 0.05 ML coverage, grow isotropically without following the ridge orientation but developing a more irregular and granular shape, as discussed below. Up to 0.30 ML, only monolayer high islands are observed with an apparent height of 2.6 ± 0.2 Å. Above 0.25 ML the out-of-elbow nucleation becomes evident (Fig. 1.b) together with the distortion of the underlying herringbone reconstruction (Fig. 2.c), thus resulting in a reduction of ordered growth of islands up to about 0.50 ML when the island alignment is almost completely lost. At the same time negligible coalescence is observed even after 0.50 ML.

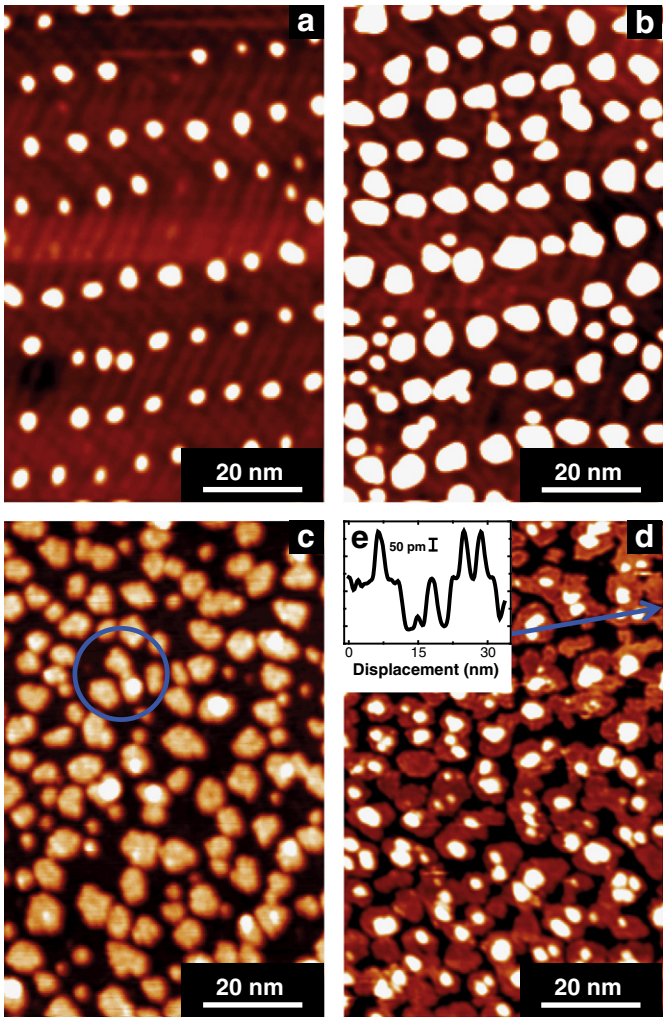

Fig. 1. Constant current STM images of increasing amount of Ti deposited onto reconstructed Au(111) surface: a) 0.05 ML (setpoint V = −0.4 V, I = 1.2 nA), b) 0.25 ML (V = −0.6 V, I = 1.1 nA), c) 0.50 ML (V = −0.5 V, I = 1.7 nA), d) 0.90 ML (V = −0.5 V, I = 0.7 nA). e) Line profile along the arrow shown in d). The circle in c) indicates coalescence among the islands and initial second layer growth. The image contrast in c) and d) has been exaggerated in order to distinguish the second layer on top of first layer of Ti islands.

Significant second layer growth on top of monolayer islands appears at coverage >0.50 ML (Fig. 1.c and d), showing the same apparent height as the first layer. Such height values do not depend on the applied bias and tunneling current.

In order to discuss growth mechanisms and island structure we report higher magnification images in Fig. 2. At 0.05 ML (Fig. 2.a) the presence of several depressions or holes mainly localized nearby Ti islands is observed, these depressions not being observed on the clean surface before evaporation of Ti. The line profile of these dark spots reveals an apparent depth of about 0.4 Å with respect to the substrate. Such features may indicate the presence of embedded Ti atoms in Au(111), as discussed below. At higher magnification we also observe that Ti islands have a granular structure, as composed of grains with a diameter of the order of 1–2 nm^2. This is quite evident at 0.65 ML (Fig. 2.d and e), even though the surface granularity of islands is a morphological feature that can be observed starting from 0.25 ML coverage and even below. Moreover, such granularity characterizes not only Ti first layer islands but also the second layer (not shown).

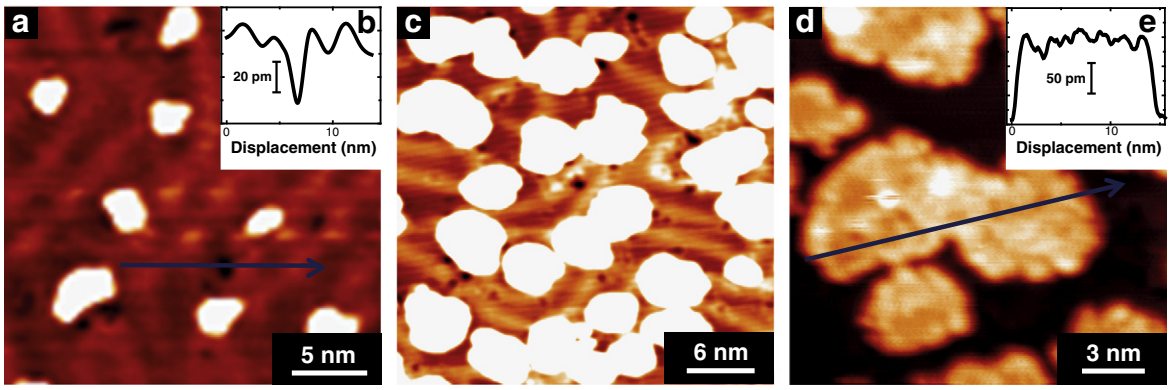

Fig. 2. Constant current STM images of increasing amount of Ti deposited onto reconstructed Au(111) surface: a) 0.05 ML (V = −0.4 V, I = 1.2 nA), c) 0.35 ML (V = −0.4 V, I = 1.2 nA), d) 0.65 ML (V = −0.4 V, I = 1.3 nA). b) and e) represent line profiles along the arrow shown in a) and d) respectively. In c) image contrast was exaggerated in order to distinguish the distortion in herringbone reconstruction.

3.2. Analysis of growth mechanisms

In order to obtain a quantitative analysis of the growth evolution of Ti islands, we performed a statistical analysis of STM images obtained at different Ti coverage.

In Fig. 3 we show the island size distribution for coverage ranging from 0.05 to 0.40 ML where the curves can be well fitted with Gaussian distributions. At the lowest coverage (0.05 ML) we reported the size distribution for separated elbow and out-of-elbow islands showing that out-of-elbow islands are typically characterized by a smaller size with respect to islands at the elbows, with an average size of 2.3 ± 1.2 nm^2 and 3.5 ± 1.0 nm^2 respectively (Fig. 3.a). This is reasonable when considering that out-of-elbow islands probably start to nucleate after saturation of elbow sites or after these reach a critical size. As the coverage is increased to 0.15 ML the mean size increases to 11 ± 4 nm^2, finally reaching 22 ± 7 nm^2 at 0.40 ML (Fig. 3.b). The size distribution becomes broader and asymmetrical, probably due to out-of-elbow nucleation in parallel with increase of in-elbow islands. The asymmetry becomes more evident at 0.40 ML where large islands (~50–100 nm^2) originating from the beginning of coalescence are present.

Quantitative information about coalescence can be obtained by an analysis of the evolution of island density (i.e. the number of islands per unit surface) as a function of total coverage, as reported in Fig. 4.a. Three different growth regions can be observed: below 0.20 ML (region I) island density slightly increases with coverage while always exceeding the elbow density (contribution of out-of-elbow sites), as already discussed; above 0.20 ML island density reaches a plateau (region II); and at approximately 0.40 ML it starts to decrease, eventually reaching the elbow density at about 0.65 ML. These observations confirm that the evolution of island density is the result of two competitive processes, nucleation of new islands dominating at low coverage and coalescence dominating at high coverages.

Since coalescence is a direct consequence of islands size growth, it is interesting to observe the evolution of average island area versus coverage, represented in Fig. 4.b. We can identify two different growth regimes separated by a threshold located at about 0.40 ML. Both regimes are characterized by a linear increase, but with different slopes, of the average area with respect to the first layer coverage; Linear fits show a three times faster increase starting from 0.40 ML and we attribute such behavior to the occurrence of coalescence among islands.

The first and second layer coverage fraction as a function of Ti total coverage is shown in Fig. 5. Up to about 0.50 ML, first layer growth is characterized by a linear increase, while after this value it starts to deviate from this behavior. Second layer appears at 0.30 ML but it starts growing significantly after 0.50 ML in correspondence of the deflection observed for the first layer. To interpret these data and to evaluate the interlayer diffusion, we can make use of rate equations in the time (or equivalently coverage) domain. Following an early work of Cohen et al. [16], the interlayer diffusion can be accounted for in the so-called *diffusive growth model*:

$$\frac{d\vartheta_n}{dt} = \frac{1}{\tau}(\vartheta_{n-1} - \vartheta_n) + J_{n+1\to n} - J_{n\to n-1}; \quad \vartheta_n(0) = 0 \tag{1}$$

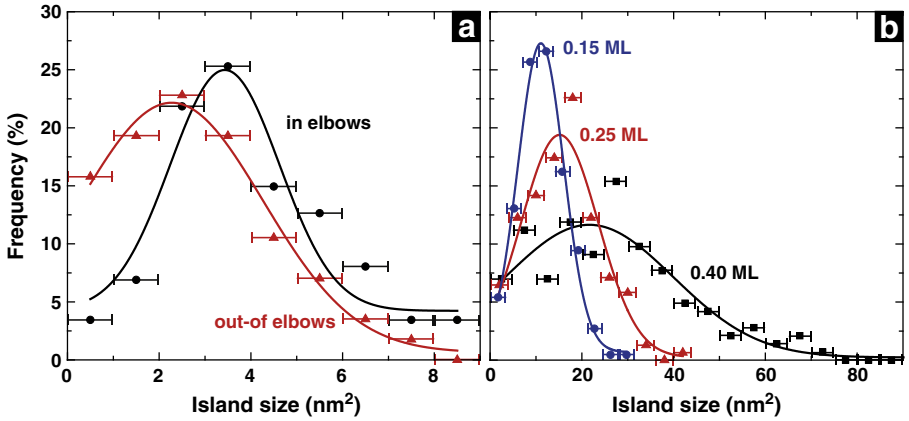

Fig. 3. a) Island size distributions for 0.05 ML coverage showing separated distributions for in-elbows and out-of-elbows islands. b) Size distributions (counting both in-elbows and out-of-elbows islands) ranging from 0.15 ML to 0.40 ML coverage. All data points are taken from the analysis of STM images and are fitted with Gaussian functions.

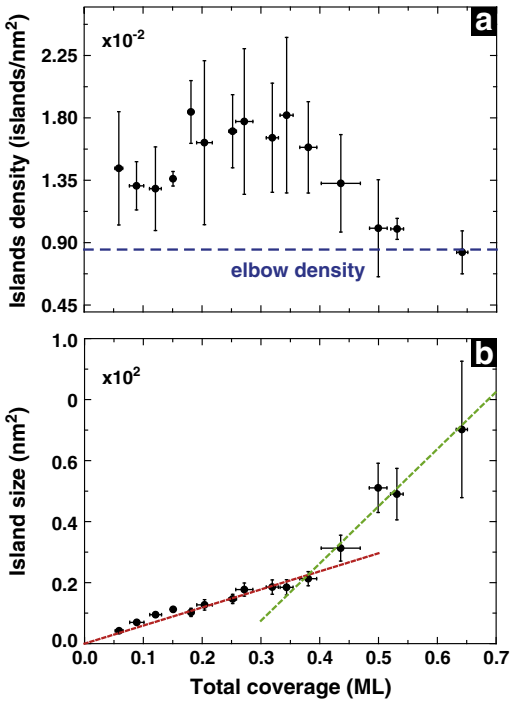

Fig. 4. a) Surface islands density as a function of total Ti coverage (black dots). The blue dashed line represents the elbows density of the gold reconstruction (8.5×10^{-3} nm^{-2} [6]). b) Islands area vs. Ti coverage (black dots). Linear fits (dashed lines) are reported to show the two different growth regimes.

where θ_n is the fraction coverage of the *n-th* layer, $1/\tau$ is the deposition rate and $J_{m \to n}$ represents the net jump rate of adatoms to the *n-th* layer from the *m-th* layer. A variety of models could be used for the last two terms [16]. We assume the jump rate from$(n+1)$th to nth layer to be proportional to the product of the available free surface on level n and the uncovered area on level $n+1$. The assumption is that once an underlying atom is covered it is not able to diffuse to the island edge. Then Eq. (1) becomes:

$$\frac{d\vartheta_n}{dt} = \frac{1}{\tau}(\vartheta_{n-1} - \vartheta_n) + k(\vartheta_{n+1} - \vartheta_{n+2})(\vartheta_{n-1} - \vartheta_n) - k(\vartheta_n - \vartheta_{n+1})(\vartheta_{n-2} - \vartheta_{n-1}) \quad (2)$$

where k is the interlayer diffusion rate (s^{-1}). Assuming a constant flux $1/\tau$ (3.3×10^{-3} ML/s, estimated from the evolution of coverage vs time), it is possible to fit the experimental data with this set of differential equations in order to optimize the k parameter. In Fig. 5 dashed lines

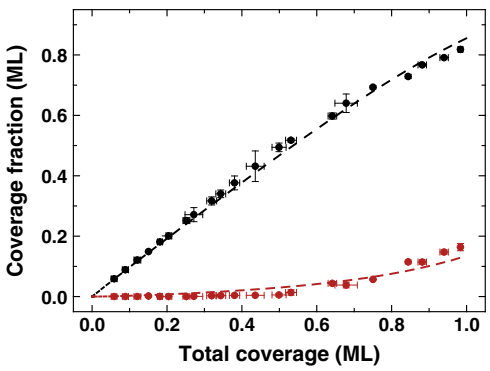

Fig. 5. First (black) and second (red) layer coverage as a function of total coverage. Dots represent the experimental data while dashed lines are the fit with the diffusive model.

represent theoretical curves where the fitting procedure gives, for the interlayer diffusion rate, a value of $k = 0.8 \times 10^{-2}$ s^{-1}. The model seems to properly account for the growth dynamics. However, it can be noticed that the experimental data related to the first layer are slightly underestimated in the range 0.40–0.60 ML, while they result overestimated at coverage >0.80 ML; vice versa for the second layer. This mismatch could be due to different causes. From a theoretical point of view, this model is based on the hypothesis of a constant interlayer diffusion rate k. A more accurate representation of layer growth processes should consider both the effective density of free adatoms that are involved in this process and the related energy barrier [17]. This barrier is related to the diffusion activation energy and to the so called *Ehrlich-Schwoebel energy*, that is the additional energy barrier encountered by an atom when diffusing from a layer to the underlying one [18,19]. The diffusive growth model is useful to understand the mechanisms governing the second layer growth, even though when increasing the coverage the Ehrlich–Schwoebel barrier may vary in a complex way, as a function of the layer coverage fraction, island size and perimeter [20].

Our results outline some important distinctive features which characterize the growth of Ti on Au(111) with respect to other metals showing the preferential nucleation on the elbows of the herringbone reconstruction. First of all we observe an early occurrence of out-of-elbow nucleation (even before 0.05 ML) with saturation of the elbows sites, while a similar condition is reached after 0.10 ML in the case of Pd/Au(111) [6] and after 0.15 ML for Fe/Au(111) [17]. In the growth of Ti this effect parallels with a retarded coalescence between islands if compared to other systems such as Pd/Au(111) where directional coalescence along the direction of elbow rows is observed [6,21]. In case of perfectly ordered nucleation at the elbows, coalescence along $[11\bar{2}]$ is expected to occur already at 0.2 ML according to growth simulations of the Fe/Au(111) system [22]. In our case, Ti island coalescence is retarded (0.40 ML) with respect to this value, probably due to the existence of other (out-of-elbow) nucleation centers even at the lowest coverages, resulting in an early onset of disordered growth, similarly to the case of Fe/Au(111), where coalescence is experimentally observed to occur at about 0.35 ML [17]. At a coverage >0.30 ML the typical size of Ti islands becomes comparable to the distance between two adjacent ridges, and further growth causes a distortion of the substrate reconstruction. This behavior is also observed in Pd for which a substantial distortion of the gold surface was observed in a similar coverage range [6], while it is markedly different from Fe and Co islands whose growth does not significantly influence the underlying reconstruction [3,4].

Second, the granular morphology and structure of islands (Fig. 2.d) appear as a distinctive feature of Ti growth since it has not been observed for other metals on Au(111), such as Pd, Fe and Co. Ti islands appear composed by an assembly of grains whose size (about 1 nm) corresponds to that of out-of-elbow islands observed at early stages. A possible explanation can be related to a relevant Ti–Au interaction competitive with Ti–Ti one. In this way desorption of Ti atoms from the edge of growing islands could be a relevant, energetically favored process beyond a critical island size, leading to formation of out-of-elbows clusters which once formed have hindered diffusion. For Fe/Au(111) we have already shown that such a process can explain the presence of out-of-elbow islands, even though Fe islands grow as triangular or diamond shaped nanocrystals [17]. Such process is expected to produce a high island density in close vicinity to already existing islands thus leading to granular morphology, since a high affinity between Ti and Au could lead Ti adatoms to bind with Au surface atoms instead of sticking to a Ti island, thus favoring the formation of aggregates composed by ultrafine grain units. Moreover we observe that titanium has been reported to have a tendency to form alloy with gold [14,23]. Such hypothesis is further supported by the observation of dark regions at 0.05 ML which may be produced by the presence of Ti atoms replacing gold atoms, possibly at sub-surface sites, as invoked for explaining similar observations reported for Pd/Au(111) [21,24,25].

3.3. Electronic properties

The STS analysis of the Ti/Au(111) system was performed up to 0.50 ML coverage and was focused on the study of the electronic properties (Local Density of States, LDOS) of first layer islands before coalescence becomes dominant. In Fig. 6 we present *dI/dV* spectra, measured over a bias range from −1.5 to 1.5 V, and acquired on top of Ti islands for different coverages. Since no significant differences in the main spectral features were observed between spectra acquired at the same coverage on Ti islands at different surface sites or with different size, we show only a single representative dI/dV curve for each investigated coverage (which is the result of averaging over many measurements on the same island as explained in the Experimental section). No 'normalization' procedure was adopted considering the limited bias range and the intensity of the observed features.

The spectra are characterized by three dominant peaks: one is in the occupied states at about −0.65 eV (α), while the other two peaks are in the unoccupied states at about 0.20 eV (β) and 0.85 eV (γ). As mentioned, the energy position of these peaks does not significantly change with respect to nucleation site, island size and position within Ti island. The only observed variation concerns their relative intensity, mainly as a function of coverage. In particular, at higher coverage the intensity of β and γ peaks decreases with respect to α peak.

Further information is provided by the analysis of differential conductivity maps at different applied bias (LDOS maps, i.e. *dI/dV* maps acquired during a constant current scan with active feedback loop). As expected, at a bias of about −0.7, 0.2 and 0.8 V (close to the energy position of Ti peaks), in differential conductivity maps we observed a brighter region in correspondence of Ti islands, while darker regions correspond to the gold substrate. This contrast is the result of the different LDOS on Ti islands at specific energies. This is nicely illustrated in Fig. 7.a and b, showing a region of Ti/Au(111) for a coverage of 0.20 ML and the corresponding LDOS map at −0.70 V, respectively. On the contrary, at −0.46 V this contrast is reversed, since the Au(111) Shockley state that has an onset at −0.46 eV [26] leads to a higher brightness in correspondence of the substrate (not shown).

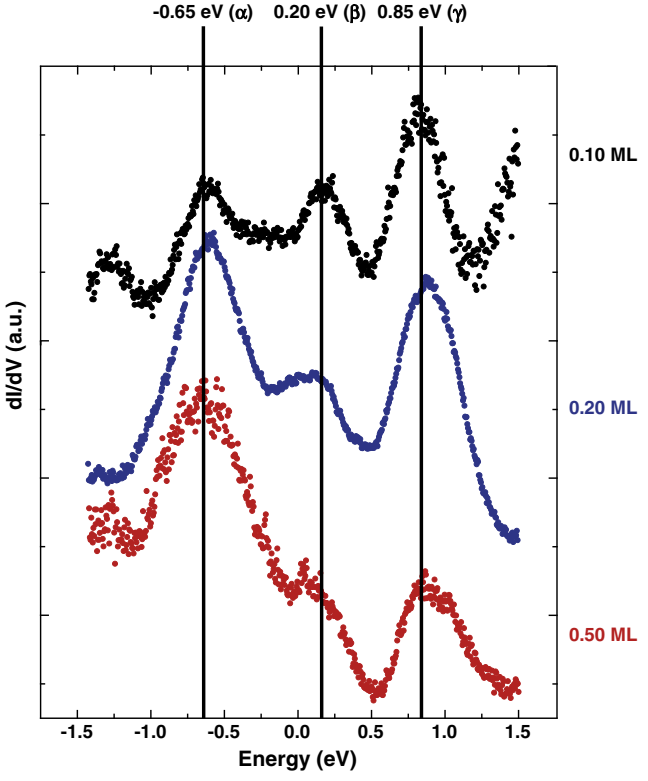

Fig. 6. Representative STS spectra (*dI/dV*) recorded at 100 K at various coverage: 0.10 ML (black dots), 0.20 ML (blue dots) and 0.50 ML (red dots).

Fig. 7.b shows regions of the substrate with the same brightness of Ti islands even if no contrast is revealed in the topographic image (blue dot in Fig. 7). In order to gain more insight, single point STS spectra for different regions of the constant current images were acquired(Fig. 7.c), i.e. on Ti islands and on the underlying substrate, to compare their electronic features. *dI/dV* curves on Ti islands are characterized by the three previously discussed dominant peaks (red curve). For the substrate regions corresponding to the darker areas in the *dI/dV* map, the Shockley peak appears modified by a prominent hump at about 0.20 eV (black curve). Moreover, the substrate regions revealing the same brightness of Ti islands in the LDOS map show a spectrum qualitatively similar to that found for Ti islands (blue curve). More in particular, for these areas it can be observed that α and γ peaks are dominant while β peak almost disappears (there is only a small hump at its energy position).

Our observations suggest the presence of a significant interaction between the deposited metal and the substrate surface. Some substrate regions, apparently belonging to Au(111) by looking at topographic images, reveal the same contrast as Ti islands in *dI/dV* maps (blue point in Fig. 7) thus possibly indicating the presence of Ti 'embedded' in the substrate. STS spectra of those regions are modified with respect to Ti islands (i.e. strong reduction of the β peak) while not showing a distinctive Shockley peak of Au(111) and even the STS spectra of the Au(111) substrate regions present modified electronic features, the Shockley peak being characterized by a shoulder at about 0.20 eV. For comparison, we reported in Fig. 7.b the clean Au(111) STS spectrum (purple dashed line).

A tentative interpretation of the STS data obtained in the different substrate regions could be related to the different physical state in which embedded (surface or subsurface) Ti would be with respect to Ti island. In the same way the modification of the Shockley peak on Au(111) could be interpreted as the result of the perturbation induced by the presence of Ti (islands or embedded in Au(111)), since it is known that due to their extreme surface localization, Shockley states of noble metals are sensitive to any surface (structural or chemical) modification, including islands and overlayers [13,27].

4. Conclusions

We performed a detailed scanning tunneling microscopy and spectroscopy study of the growth of titanium on the Au(111) reconstructed surface. The initial preferential nucleation of Ti islands at the elbows of the herringbone reconstruction is accompanied by out-of-elbow nucleation starting from the lowest coverage investigated (~0.05 ML). Increasing the coverage, the island size increases with coalescence starting at about 0.40–0.50 ML, retarded with respect to other systems, such as Pd, while second layer features appear above 0.50 ML. Ti islands are characterized by a peculiar granular structure (found also for the second layer) suggesting that islands are indeed made of small grains.

STS measurements revealed that, up to 0.50 ML, Ti islands are characterized by three dominant electronic features around Fermi energy, whose energy positions do not change as a function of coverage. *dI/dV* maps reveal the presence of some substrate regions with electronic features similar to Ti islands, and local STS spectra of these regions show a strong correlation with those revealed for Ti islands. Such observations and the modification of the Au(111) surface Shockley state suggest an important interaction between Ti and the Au surface.

Our detailed study of morphological and electronic properties of Ti nanoislands deposited on Au(111) shows that Ti growth displays peculiar features with respect to other elements belonging to the same group of atoms undergoing preferential nucleation at the elbows of Au(111). Such characteristics are important both when adopting Ti/Au(111) as a model system for catalytic studies and when considering subsequent oxidation and formation of TiO_2 nanoislands and layers [14,28] which represent an interesting system for surface science investigations of many application-relevant processes such as photocatalysis and photovoltaics.

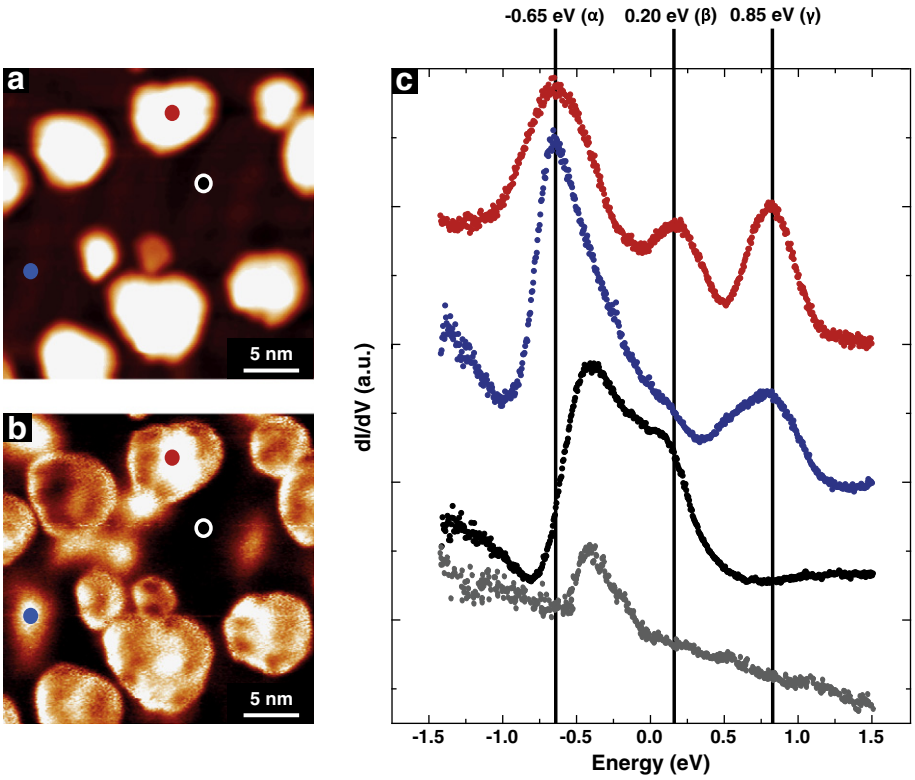

Fig. 7. a) Constant current STM image (V = −0.7 V, I = 1.0 nA) of 0.20 ML of Ti on Au(111). b) Corresponding *dI/dV* map of the same area reported in a) at a bias voltage of −0.7 V. c) STS spectra of different regions: Ti island (red dots) and substrate with different contrast in *dI/dV* map (blue and black dots). STS spectrum on the clean Au(111) is reported in grey for reference.

References

[1] Q. Yi, W. Yu, Microchim. Acta 165 (2009) 381.
[2] J.V. Barth, H. Brune, G. Ertl, R.J. Behm, Phys. Rev. B 42 (1990) 9307.
[3] J.A. Stroscio, D.T. Pierce, R.A. Dragoset, P.N. First, J. Vac. Sci. Technol. A 104 (1992) 1981.
[4] B. Voigtländer, G. Meyer, N.M. Amer, Phys. Rev. B 44 (1991) 10354.
[5] D.D. Chambliss, R.J. Wilson, S. Chiang, Phys. Rev. Lett. 66 (1991) 1721.
[6] C.S. Casari, S. Foglio, F. Siviero, A. Li Bassi, M. Passoni, C.E. Bottani, Phys. Rev. B 79 (2009) 195402.
[7] M.Ø. Pedersen, S. Helveg, A. Ruban, I. Stensgaard, E. Lægsgaard, J.K. Nørskov, F. Besenbacher, Surf. Sci. 426 (1991) 395.
[8] M.M. Biener, J. Biener, R. Schalek, C.M. Friend, Surf. Sci. 594 (2005) 221.
[9] J. Biener, E. Farfan-Arribas, M. Biener, C.M. Friend, R.J. Madix, J. Chem. Phys. 123 (2005) 094705.
[10] W.G. Cullen, P.N. First, Surf. Sci. 420 (1999) 53.
[11] A.W. Stephenson, C.J. Baddeley, M.S. Tikhov, R.M. Lambert, Surf. Sci. 398 (1998) 172.
[12] I. Chado, C. Goyhenex, H. Bulou, J.P. Bucher, Phys. Rev. B 69 (2004) 085413.
[13] N. Nicoara, E. Roman, J.M. Gomez-Rodrigez, J.A. Martin-Gago, J. Mendez, Org. Electron. 7 (2006) 287.
[14] D.V. Potapenko, R.M. Osgood, Nano Lett. 9 (2009) 2378.
[15] A. Li Bassi, C.S. Casari, D. Cattaneo, F. Donati, S. Foglio, M. Passoni, C.E. Bottani, P. Biagioni, A. Brambilla, M. Finazzi, F. Ciccacci, L. Duò, Appl. Phys. Lett. 91 (2007) 173120.
[16] P.I. Cohen, G.S. Petrich, P.R. Pukite, G.J. Whaley, A.S. Arrott, Surf. Sci. 216 (1989) 222.
[17] F. Donati, A. Mairov, C.S. Casari, M. Passoni, A. Li Bassi, Surf. Sci. 606 (2012) 702.
[18] G. Ehrlich, F.G. Hudda, J. Chem. Phys. 44 (1966) 1039.
[19] R.L. Schwoebel, J. Appl. Phys. 40 (1969) 614.
[20] S.Y. Kim, I.H. Lee, S. Jun, Phys. Rev. B 76 (2007) 245408.
[21] C.S. Casari, S. Foglio, M. Passoni, F. Siviero, C.E. Bottani, A. Li Bassi, Phys. Rev. B 84 (2011) 155441.
[22] P. Ohresser, N.B. Brookes, S. Padovani, F. Scheurer, H. Bulou, Phys. Rev. B 64 (2001) 104429.
[23] L. Murray, Bull. Alloy Phase Diagr. 4 (1983) 278.
[24] A. Baber, H. Tierney, E.C.H. Sykes, ACS Nano 4 (2010) 1637.
[25] G. Fratesi, J. Phys. Condens. Matter 23 (2011) 015001.
[26] K. Schouteden, P. Lievens, C. Van Haesendonck, Phys. Rev. B 79 (2009) 195409.
[27] D. Malterre, B. Kierren, Y. Fagot-Revurat, S. Pons, A. Tejeda, C. Didiot, H. Cercellier, A. Bendounan, New J. Phys. 9 (2007) 391.
[28] C. Wu, M.S.J. Marshall, M.R. Castell, J. Phys. Chem. C 115 (2011) 8643.